JMB

ELSEVIER

Comparative Analysis of Membrane-Associated Fusion Peptide Secondary Structure and Lipid Mixing Function of HIV gp41 Constructs that Model the Early Pre-Hairpin Intermediate and Final Hairpin Conformations

Kelly Sackett[1], Matthew J. Nethercott[1], Raquel F. Epand[2], Richard M. Epand[2], Douglas R. Kindra[1], Yechiel Shai[3] and David P. Weliky[1]*

[1]*Department of Chemistry, Michigan State University, East Lansing, MI 48824, USA*

[2]*Department of Biochemistry and Biomedical Science, McMaster University, Hamilton, Ontario, Canada L8N 3Z5*

[3]*Department of Biological Chemistry, Weizmann Institute of Science, Rehovot 76100, Israel*

Fusion between viral and host cell membranes is the initial step of human immunodeficiency virus infection and is mediated by the gp41 protein, which is embedded in the viral membrane. The ~20-residue N-terminal fusion peptide (FP) region of gp41 binds to the host cell membrane and plays a critical role in fusion catalysis. Key gp41 fusion conformations include an early pre-hairpin intermediate (PHI) characterized by extended coiled-coil structure in the region C-terminal of the FP and a final hairpin state with compact six-helix bundle structure. The large "N70" (gp41 1–70) and "FP-Hairpin" constructs of the present study contained the FP and respectively modeled the PHI and hairpin conformations. Comparison was also made to the shorter "FP34" (gp41 1–34) fragment. Studies were done in membranes with physiologically relevant cholesterol content and in membranes without cholesterol. In either membrane type, there were large differences in fusion function among the constructs with little fusion induced by FP-Hairpin, moderate fusion for FP34, and very rapid fusion for N70. Overall, our findings support acceleration of gp41-induced membrane fusion by early PHI conformation and fusion arrest after folding to the final six-helix bundle structure. FP secondary structure at Leu7 of the membrane-associated constructs was probed by solid-state nuclear magnetic resonance and showed populations of molecules with either β-sheet or helical structure with greater β-sheet population observed for FP34 than for N70 or FP-Hairpin. The large differences in fusion function among the constructs were not obviously correlated with FP secondary structure. Observation of cholesterol-dependent FP structure for fusogenic FP34 and N70 and cholesterol-independent structure for non-fusogenic FP-Hairpin was consistent with membrane insertion of the FP for FP34 and N70 and with lack of insertion for FP-Hairpin. Membrane insertion of the FP may therefore be associated with the early PHI conformation and FP withdrawal with the final hairpin conformation.

© 2010 Elsevier Ltd. All rights reserved.

Edited by J. Bowie

Corresponding author. E-mail address: weliky@chemistry.msu.edu.

Introduction

The human immunodeficiency virus (HIV) infects host cells through a process of membrane fusion directed by the viral membrane protein gp41. In the unactivated native state, trimeric gp41 is shrouded by three surface gp120 protein subunits on the viral membrane surface (Fig. 1a). Activation occurs by binding of gp120 to specific target cell receptors, with subsequent interaction of gp41 with the target cell membrane.[1,2] The ~180-residue ectodomain of gp41 lies outside the virus and undergoes conformational change, which is correlated with membrane fusion.[3] The ectodomain is composed of an apolar N-terminal fusion peptide (FP) region, N- and C-terminal heptad repeat regions (NHR and CHR, respectively) separated by a loop, and a membrane-proximal external region (MPER, Fig. 2a). It is thought that the FP binds to target cell membranes in an early activated gp41 fusion conformation termed the pre-hairpin intermediate (PHI), with extended structure C-terminal of the FP and exposed CHR and NHR regions (Fig. 1b).[1–4] Parallel coiled-coil NHR organization in the N-terminal half of the PHI (N-PHI) maintains gp41 trimeric assembly and is the only structural element characterized *in vivo* for the PHI gp41 conformation.[5] Gp41-mediated fusion can be arrested by small molecules or gp41-derived peptides and the N-PHI structure has been a successful target of entry inhibitors.[6] In the absence of inhibitors, gp41 folds to its final hairpin conformation (Fig. 1c). The hairpin conformation is based on high-resolution structures of soluble parts of the gp41 ectodomain that contain the NHR and CHR and has parallel NHR coiled-coil structure, with CHR regions packing antiparallel along the three hydrophobic coiled-coil grooves in six-helix bundle (SHB) fashion with high thermostability (Fig. 1c).[7–9]

The existing high-resolution gp41 structures lack the FP region, and fusion models generally show FP binding to the target membrane in the PHI conformation (Fig. 1b and c).[9,10] Mutational studies of the FP region in gp41 show that the FP plays a critical role in virus/host cell fusion. For example, mutant V2E gp41 displays trans-dominance when co-expressed with wild-type gp41, which suggests that FP-mediated gp41 assembly is relevant to fusion.[11] Structure–function analyses of gp41 fragment constructs that contain the FP show that many of these constructs catalyze vesicle fusion and that the FP induces oligomerization of gp41 trimers.[12–18] There is good correlation between loss of *in vivo* fusion by specific FP mutations and reduction of inter-vesicle lipid mixing induced by gp41 constructs with these mutations, which supports the relevance of these constructs for understanding the structure and function of gp41.[11,12]

The N-terminal FP is minimally assembled into trimers by gp41 trimeric coiled-coil and SHB folds (Figs. 1b and c and 2c and d). Peptides corresponding to the FP(1–23) region alone aggregate in aqueous solution near neutral pH, but monomeric FP can be achieved with addition of nonnative C-terminal lysines.[19] The oligomerization/aggregation state of FP in aqueous solution has some impact on fusogenicity, and small FP oligomers are more fusogenic than either FP monomers or large FP aggregates. For FP:total lipid molar ratio = 0.01, the relative final extents of lipid mixing induced by FP monomers, small oligomers, and large aggregates are 1.0:1.5:0.5. The particular significance of FP trimers relative to monomers was demonstrated by functional comparison between FP monomer and FP trimer made by chemical cross-linking.[17] Neither FP monomer nor FP trimer aggregates in aqueous solution, and relative to FP monomer, FP trimer induces inter-vesicle lipid mixing at 15- to 40-fold higher rate and with half the activation energy. The N70 protein (Fig. 2a and c) contains the FP and most of the NHR, which is the trimeric auto-oligomerization motif for gp41,[18,20] and its lipid mixing function is comparable to that of the FP trimer.[16,17,21,22] N70 binds strongly to the NC-1 monoclonal antibody, which recognizes the trimeric NHR coiled coil (Figs. 1b and 2a and c).[18,23] Taken together, these results indicate the following: (1) a significant fraction of N70 in aqueous solution is organized as trimers, reproducing the N-terminal half of the PHI or N-PHI (Fig. 1b), and (2) trimeric assembly of FPs by NHRs is the basis for rapid and extensive membrane fusion by N70. In very large contrast
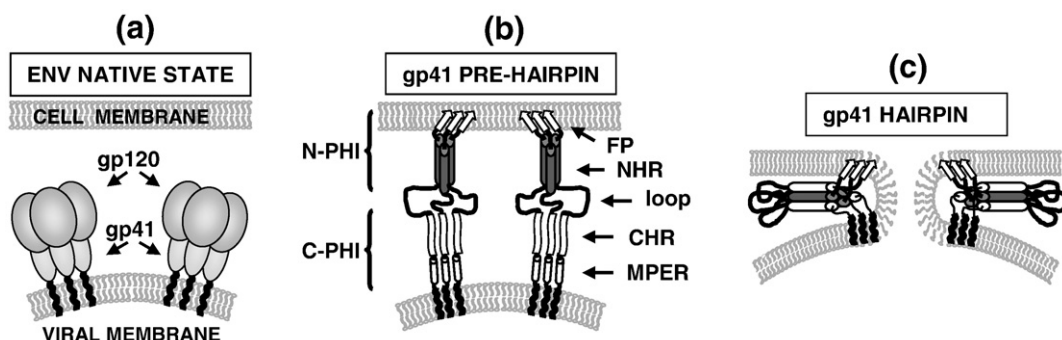

Fig. 1. (a–c) HIV fusion model. (b and c) Gp120 is not shown in order to focus on gp41 organization. The FP region is indicated using arrows.
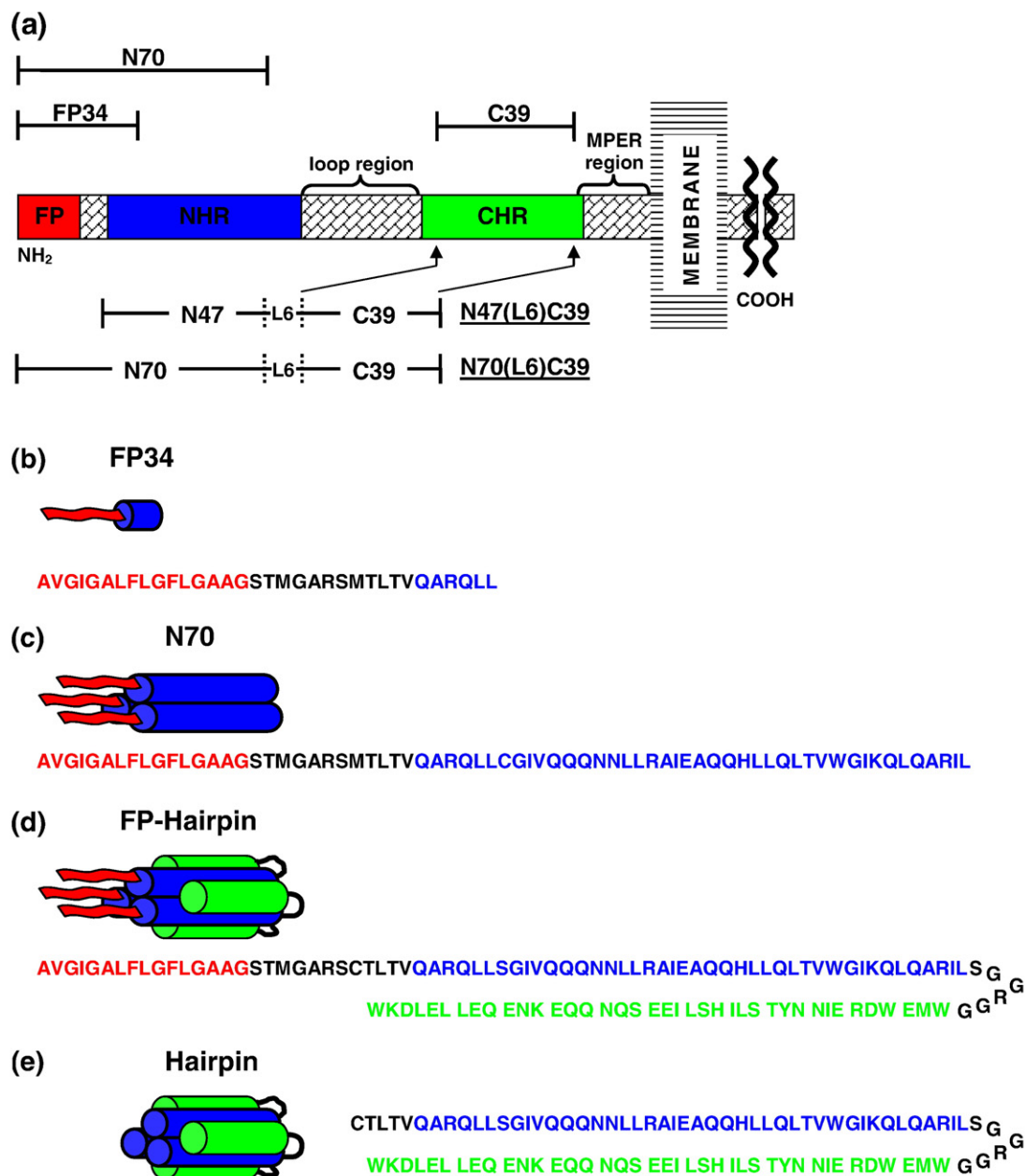
Fig. 2. (a) Schematic of the HIV-1 gp41 ectodomain. Primary functional regions are designated by colored boxes and additional functional regions are specified above in braces. Above and below in brackets are the gp41 fragments under study. (b–e) Structural representation of FP34, N70, FP-Hairpin [N70(L6)C39], and Hairpin [N47(L6)C39], respectively, in aqueous solution, with primary sequence below each, color coded to match functional regions in (a). FP34 is shown as a monomer but likely aggregates nonspecifically in aqueous solution. The alignment of the NHR and CHR sequences approximately reflects their alignment in crystal structures of NHR and CHR fragment peptides.

to rapid lipid mixing at physiologic pH induced by FP trimer and N70, negligible lipid mixing is induced by the FP-Hairpin construct, which models the final gp41 fusion conformation (Figs. 1c and 2d).[22] FP-Hairpin contains the FP, NHR, a short loop, and the CHR, with highly thermostable hairpin assembly of the NHR and CHR (Fig. 2a and d). In fact, addition of FP-Hairpin to a solution containing membrane vesicles and N70 or the FP34 fragment (Fig. 2a and b) stops lipid mixing. Similar inhibition was observed for Hairpin, which lacks

the FP (Fig. 2a and e), and strongly suggests that viral fusion at physiologic pH is arrested by the final hairpin conformation of gp41.[22] Constructs similar to Hairpin with SHB structure also inhibit cell–cell fusion.[24] The lipid mixing results of N70 and FP-Hairpin support a model in which membrane fusion at physiologic pH is catalyzed by the early PHI conformation and stopped by the final hairpin conformation with host cell viability improved by the hairpin stabilization of the fused membrane.[3,22]

There has been significant structural study of the membrane-associated FP in the absence of the rest of gp41. A high-resolution liquid-state nuclear magnetic resonance (NMR) structure of monomeric FP in detergent micelles showed a continuous α-helix from Ile4 to Met19.[25] In some contrast, a high-resolution solid-state NMR (SSNMR) structure showed continuous β-sheet conformation from residues Ala1 through Gly16 with about half of the FPs forming intermolecular antiparallel β-sheet structure with registries with adjacent strand crossing near Phe8 and Leu9.[26] This latter structure was obtained in membranes whose cholesterol content (30 mol%) was comparable to that of membranes of host cells of HIV.[27] In membranes that lacked cholesterol, there was a mixture of helical and β-sheet FP conformations.[21] The secondary and tertiary structures of the previously described FP trimer in membranes were similar to those of FP monomer including cholesterol dependence.[21] Lipid mixing induced by FP or FP trimer occurs for vesicles with or without cholesterol, which suggests that both helical and β-sheet conformations are fusogenic.[17] There is no consensus on this idea with other proposals that β-sheet FP is fusogenic while helical FP is not,[12] that helical FP is fusogenic while β-sheet FP is not,[14] or that neither helical nor β-sheet FP is fusogenic with fusion activity instead directed by an unstructured intermediate.[15] An alternate experimentally supported structure–function model is correlation of increased FP fusogenicity with deeper membrane insertion of the FP.[28] This correlation would hold for both helical and β-sheet FP conformations.

In contrast to the FP, there has been relatively little structural study of larger membrane-associated gp41 constructs that contain the FP and such data are needed to understand the membrane fusion mechanism. The present study addresses this issue with SSNMR analysis of the Leu7 conformation in the FP in membrane-associated N70 and FP-Hairpin along with comparison to the shorter FP34 fragment. Earlier lipid mixing studies with these three constructs were done in membranes with cholesterol and new lipid mixing data are presented in membranes without cholesterol.[22] One strength of the present study is that the sample preparation method for SSNMR structural analysis is very similar to the lipid mixing assay, which allows for more direct comparison of structural and functional results.

Results and Discussion

SHB formation

In order for FP-Hairpin to be a model for gp41 in the final thermostable SHB fusion conformation (Fig. 2d), the SHB structure should remain intact with the appended FP and adjacent polar region. The corollary Hairpin construct is a useful model for analyzing SHB structure since it contains only NHR and CHR regions that are connected by a minimal loop (Fig. 2a and e) analogous to previously described SHB constructs.[7–9,18] Previous circular dichroism (CD) spectra of Hairpin in aqueous solution and non-denaturing detergent solution showed folded tertiary structure and complete helicity of the NHR and CHR regions, which was consistent with the helical content of the SHB crystal structures.[7–9,22] In these structures, helical conformation and trimerization are correlated because the trimer of NHR helices is a leucine zipper and because higher-order aggregation of trimers is inhibited by packing of hydrophobic side chains of the three CHR helices against hydrophobic side chains on the exterior of the NHR leucine zipper. No melting was observed by CD up to 95 °C, indicating that the Hairpin fold is highly thermostable, which is consistent with the efficient shielding of hydrophobic side chains from water in this fold.[22] Very
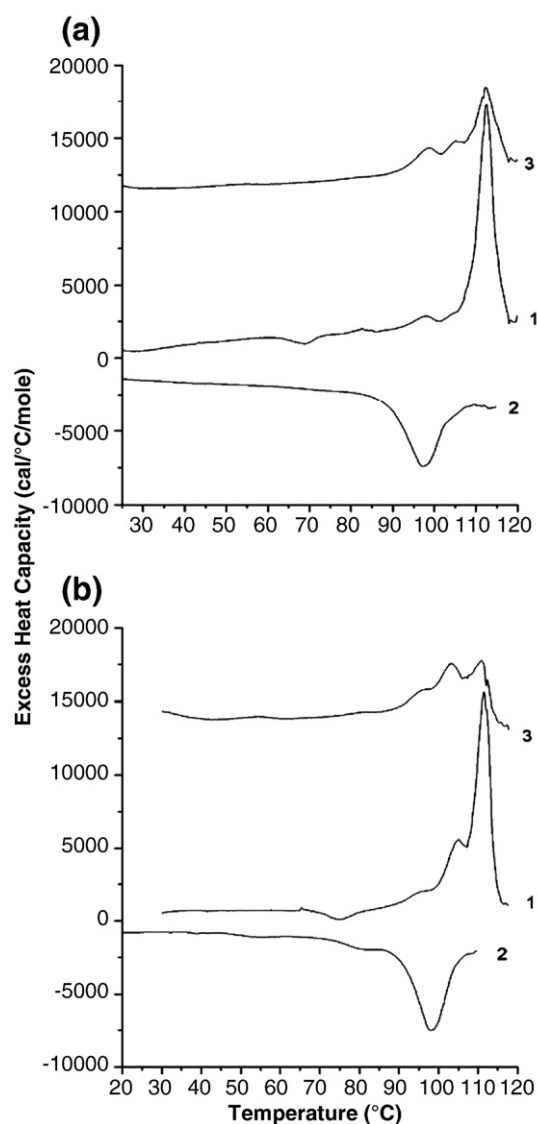
Fig. 3. DSC thermograms of Buffer-solubilized (a) 100 μM Hairpin and (b) 80 μM FP-Hairpin. Traces 1 and 3 represent the first and second heating scans, and trace 2 is the intervening cooling scan.

Table 1. Thermodynamic parameters derived from DSC analysis of FP-Hairpin and Hairpin

Sample	T_m (°C)[a]	ΔH_{cal} (kcal/mol)[b]	ΔH_{vH} (kcal/mol)[b]	$CU = \Delta H_{vH}/\Delta H_{cal}$[c]
Hairpin (100 μM)	112.4	68	240	3.5
Hairpin (25 μM)	111.4	59	230	3.9
FP-Hairpin (80 μM)	111.3	63	260	4.1
FP-Hairpin (20 μM)	111.0	56	270	4.8

[a] Estimated uncertainty is ±0.2 °C.
[b] Estimated uncertainty is ±10% for 80- or 100-μM samples and ±20% for 20- or 25-μM samples.
[c] Cooperative unfolding parameter.

high helicity and thermostability as well as folded tertiary assembly were also observed by CD for FP-Hairpin and were consistent with retention of the SHB with the appended FP.

The present study provides additional differential scanning calorimetry (DSC) evidence for the SHB fold in Hairpin and FP-Hairpin. Figure 3 shows DSC thermograms for Hairpin and FP-Hairpin in "Buffer" [10 or 20 mM formate buffer, 200 μM tris (2-carboxyethyl)phosphine hydrochloride] at pH 3.0 for two cycles of heating (traces 1 and 3) and one cycle of cooling (trace 2), and the derived calorimetric parameters are listed in Table 1. Hairpin and FP-Hairpin are comparably hyperthermostable with melting temperature $T_m \approx 112$ °C during the first heating cycle. The FP-Hairpin trace has an additional small peak at ∼105 °C. The T_m values are consistent with retention of helicity up to 95 °C observed in the CD experiments and strongly indicate that the SHB structure is not greatly affected by the FP. The calorimetric enthalpies from the first heating cycles are $\Delta H_{cal} \approx 65$ kcal/mol. Both proteins exhibit partial renaturation upon cooling as evidenced by an exothermic peak at ∼97 °C during the cooling cycle and by endothermic peaks in the 100–112 °C range during the second heating cycle. Thermograms with similar overall appearances were obtained at 4-fold lower protein concentration with very similar T_m values and similar ΔH_{cal} values (Table 1). For Hairpin and FP-Hairpin, the van't Hoff enthalpy $\Delta H_{vH} \approx 250$ kcal/mol is much higher than

ΔH_{cal}.[29] The ΔH_{vH} is reflective of the temperature dependence of the equilibrium constant of the unfolding reaction and of the number of molecules cooperatively unfolding, for example, "*n*" for a folded oligomer of *n* Hairpin or FP-Hairpin molecules changing to *n* monomeric unfolded molecules. The cooperative unfolding parameter $CU = \Delta H_{vH}/\Delta H_{cal}$ serves as a measure of *n* and is in the range of 3–5, which is generally consistent with trimer formation.

SHB formation in Hairpin and FP-Hairpin is further supported by the similar $T_m \approx 110$ °C and $CU \approx 3$ determined for gp41 constructs containing residues approximately between 25 and 150.[30–32] These constructs contained the native loop region between the NHR and CHR; thus, neither the sequence nor the length of the loop significantly impacts SHB stability. Removal of the loop reduces stability as evidenced by $T_m \approx 81$ °C in the thermograms of SHBs formed by an equimolar mixture of HIV gp41 NHR and CHR peptides.[18] Overall, the DSC data for Hairpin and FP-Hairpin in pH 3.0 Buffer support hyperthermostable SHB formation in both constructs.

Secondary structure of FP34 by SSNMR spectroscopy

Figure 4 shows rotational-echo double-resonance (REDOR)-filtered ^{13}C SSNMR spectra of three differently labeled FP34/PC (phosphatidylcholine):PG (phosphatidylglycerol):chol (cholesterol) samples

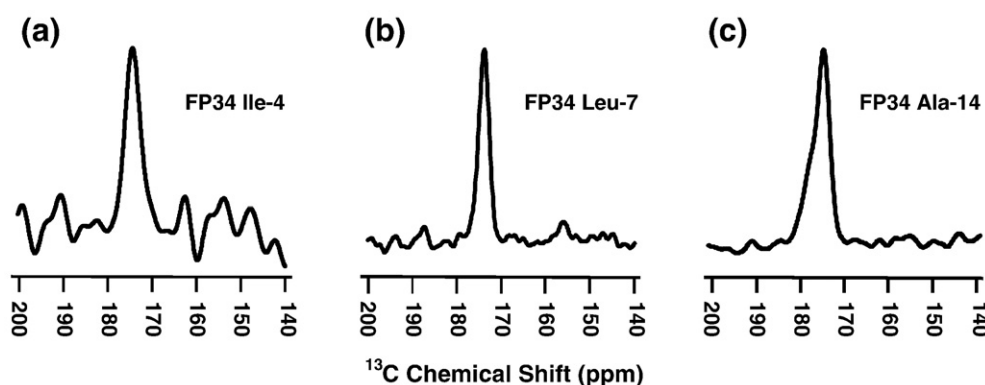**Fig. 4.** SSNMR REDOR difference spectra representing filtered (a) Ile4, (b) Leu7, or (c) Ala14 ^{13}CO signal for FP34 in PC:PG:chol membranes. The FP34:lipid molar ratio was (a and c) 1:40 or (b) 1:25. Each spectrum was processed with 200 Hz Gaussian line broadening and baseline correction and represents the sum of (a) 78,016, (b) 57,136, or (c) 134,384 $S_0 - S_1$ scans.

where FP34 includes the apolar 1–16 residues and the polar 17–34 residues of gp41 (Fig. 2a and b). The PC:PG:chol 8:2:5 molar composition reflects important aspects of the membrane composition of host cells of HIV including a large fraction of PC lipids, a small fraction of negatively charged lipids, and a significant fraction of cholesterol.[27] The NMR data were collected as separate "S_0" and "S_1" acquisitions where S_0 is the sum of all of the ^{13}C signals in the sample and S_1 has selective attenuation of the signal from the labeled ^{13}CO nucleus in FP34. In each of the Fig. 4 NMR spectra, the displayed $S_0 - S_1$ difference is due to labeled Ile4, Leu7, or Ala14 ^{13}CO signal with quantitative attenuation of natural abundance ^{13}C signal.[19] Each of the spectra is unimodal, and the peak chemical shifts are 174.4, 173.9, and 174.7 ppm, respectively (Table 2). The ^{13}CO shift is sensitive to local conformation, and there is very good agreement between the FP34 shifts and the respective 174.5-, 174.2-, and 174.9-ppm shifts of a shorter FP construct, residues 1–23, associated with membranes that contained cholesterol.[26] This agreement is important because correlations can then be made with the high-resolution structural model for this construct based on a large amount of SSNMR data. This model shows intermolecular antiparallel β-sheet structure with adjacent strand crossing near Phe8 and Leu9, that is, an antiparallel β-sheet formed from residues 1–16.[26]

The Ile4, Leu7, and Ala14 ^{13}CO shifts of FP34 in cholesterol-containing membranes can also be compared to the respective 177.1-, 179.3-, and 179.3-ppm shifts of a residue 1–30 FP construct bound to SDS detergent micelles. In SDS, this construct is monomeric and has continuous α-helical structure between residues 4 and 19.[25] The large differences between the shifts in SDS detergent and cholesterol-rich membranes support non-helical structure for the FP region in the membrane samples. Further support for β-sheet structure is obtained from comparison with the shifts of a database of proteins of known structure.[33] The normal distributions for helical or β-strand conformations are described by peak shift (standard deviation) in parts per million units: Ile, helical, 177.8 (1.3) and β-strand, 174.9 (1.4); Leu, helical, 178.5 (1.3) and β-strand, 175.7 (1.5); and Ala, helical, 179.4 (1.3) and β-strand, 176.1 (1.5).

The site-specific detection of β-sheet structure in FP34 by SSNMR is consistent with the previous report of predominant β-sheet structure in the 1–16 region based on infrared (IR) spectra of FP34 associated with cholesterol-containing membranes.[34] The SSNMR and IR sample preparation methods

were quite different; hence, the β-sheet structure likely represents the equilibrium rather than a kinetically trapped state. SSNMR samples were prepared by mixing an aqueous solution of FP34 and an aqueous solution of large unilamellar vesicles (LUVs), whereas the IR samples were prepared by co-solubilization of FP34, lipid, and cholesterol in organic solvent followed by solvent evaporation and then vapor phase hydration. A shorter FP(1–23) fragment was also studied by IR using samples prepared with an aqueous method and by SSNMR using a sample prepared with initial organic cosolubilization.[12,19] Detection of β-sheet structure in both cases provides additional support for the equilibrium nature of the β-sheet FP structure in cholesterol-containing membranes. The sample preparation method of the present SSNMR study was chosen because it likely mimics the initial interaction of gp41 with target cells and because it is very similar to the functional lipid mixing assay.

Comparison between local FP secondary structure and lipid mixing fusion function for FP34, N70, and FP-Hairpin in membranes with and without cholesterol

The FP34, N70, and FP-Hairpin constructs all contain the FP region (Fig. 2). FP34 lacks both the NHR and CHR, N70 has the NHR and is a model for the PHI gp41 conformation, and FP-Hairpin has both the NHR and CHR and is a model for the SHB gp41 conformation. Figure 5a1–a3 displays the REDOR-filtered spectra of each of the three constructs associated with PC:PG:chol membranes, and Fig. 5a4 displays representative lipid mixing traces showing the large differences in fusogenicity among the constructs at physiologic pH. FP34 induces lipid mixing at a moderate rate, which contrasts with the very rapid rate of N70 and the very slow rate of FP-Hairpin. For the spectra in Fig. 5, the Leu7 ^{13}CO/Phe8 ^{15}N labeling resulted in selective detection of the Leu7 ^{13}CO signal, which served as a probe of the conformation at the center of the FP region. The spectrum of the FP34 sample is unimodal with a peak shift of 174 ppm that corresponds to β-sheet conformation as discussed earlier. The spectra of N70 and FP-Hairpin are bimodal with peak shifts of 174 and 178 ppm. The 174 ppm shift is very close to the peak shift of the FP34 sample and is assigned to molecules with β-sheet conformation. The 178-ppm shift is very similar to the Leu7 ^{13}CO peak shift in a trimeric FP construct in PC:PG membranes.[35] In this sample, the Leu7 ^{13}CO–Phe-11 ^{15}N distance was measured by SSNMR to be 4.1 Å, which is the expected value of regular α-helical structure. The 178-ppm shift is also similar to the Leu7 ^{13}CO shift observed for α-helical FP in detergent micelles and correlates much better to the database distribution of helical Leu ^{13}CO shifts than to the distribution of β-strand shifts.[25,33] The relative intensities of the 174- and 178-ppm signals are therefore reflective of the respective populations of protein with β-sheet and α-helical Leu7 conformations. The ordering of

Table 2. REDOR-filtered peak ^{13}CO chemical shifts of FP34 in PC:PG:chol

Residue	Peak shift (ppm)	Secondary structure[a]
I4	174.4	β-Sheet
L7	173.9	β-Sheet
A14	174.7	β-Sheet

[a] There is ≤0.3 ppm difference with the corresponding ^{13}CO shift of an FP(1–23) fragment with known β-sheet structure.[26]
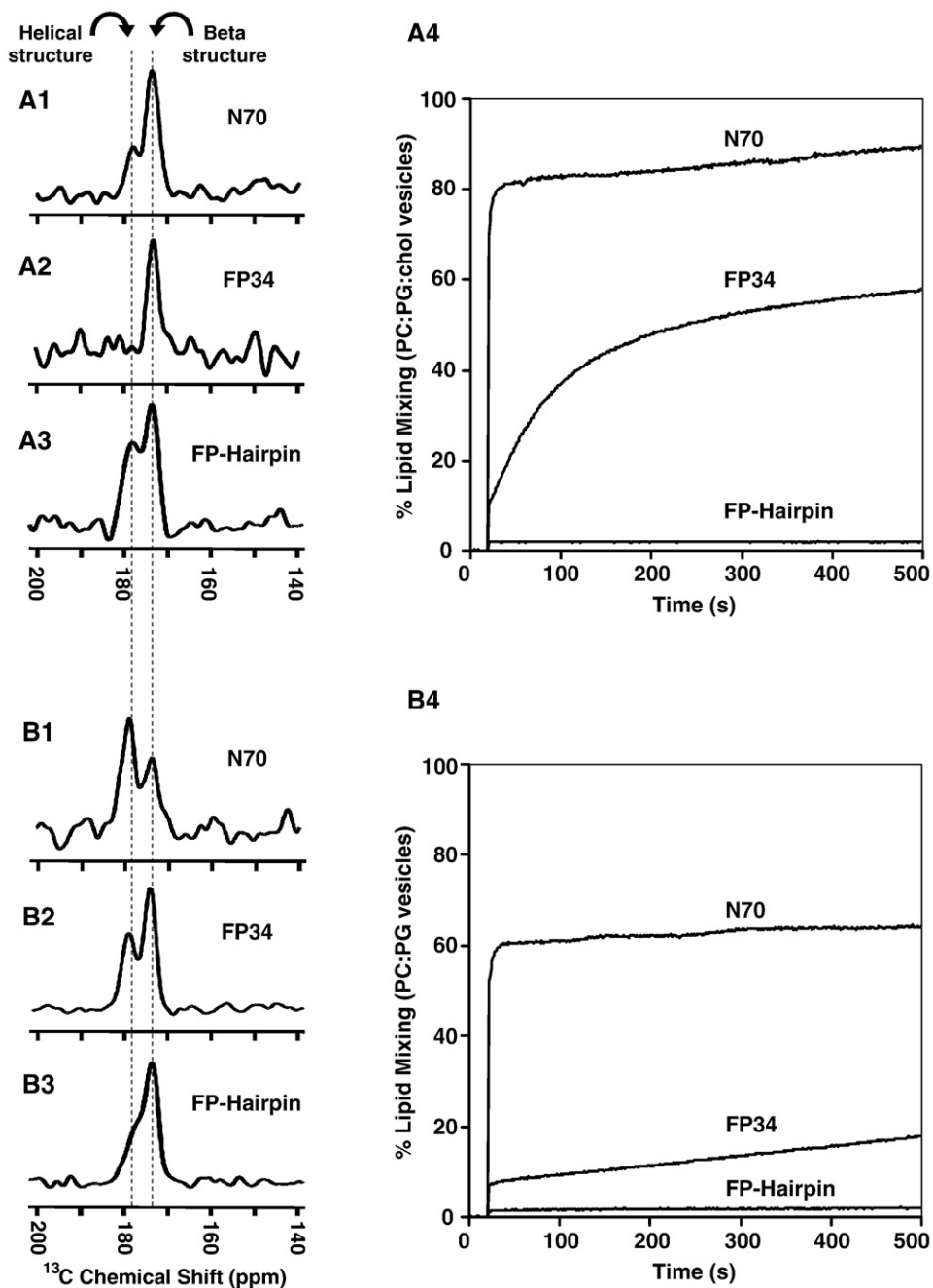
Fig. 5. REDOR difference spectra representing filtered Leu7 [13]CO signal for (a1) N70, (a2) FP34, or (a3) FP-Hairpin in PC:PG:chol membranes and (a4) lipid mixing induced between PC:PG:chol vesicles. (b1)–(b4) are identical with (a1)–(a4), except that the membrane composition is PC:PG without cholesterol. The protein:lipid molar ratios in the NMR samples were (a1) 1:40, (a2) 1:40, (a3) 1:40, (b1) 1:55, (b2) 1:25, or (b3) 1:30. Each spectrum was processed with 200 Hz Gaussian line broadening and baseline correction and represents the sum of (a1) 76,832, (a2) 200,000, (a3) 97,669, (b1) 144,176, (b2) 51,152, or (b3) 76,128 $S_0 - S_1$ scans. Broken lines are at the peak chemical shifts and are assigned to β-sheet or helical conformation. In the lipid mixing assay, time = 20 s corresponds to addition of the protein solution to the vesicle solution, the dead time was ~5 s, and the protein:lipid molar ratios were 1:50 (N70 or FP34) and 1:33 (FP-Hairpin).

the constructs in terms of relative helical population is FP34 < N70 < FP-Hairpin, and as shown in Fig. 5a4, the ordering in terms of lipid mixing function is FP-Hairpin < FP34 < N70. Comparison of the orderings does not show an obvious correlation between FP secondary structure and fusion function. Appending the NHR or the SHB does change the FP conforma-

tional populations, but the large differences in fusion function are likely due to factors other than FP conformation.

The ~30 mol% cholesterol of the PC:PG:chol (8:2:5) mixture was chosen because the membranes of HIV and the membranes of host cells of HIV contain ~45 and ~30 mol% cholesterol, respectively.[27] Some

earlier structural and functional studies of shorter FP fragments from HIV as well as FP fragments from other viruses have been carried out in detergent or membrane compositions without cholesterol.[2,13,17,25] Lipid mixing was induced by the HIV FP for vesicles with or without cholesterol, and there was a positive correlation between relative population of β-sheet FP and cholesterol content.[17,21] For PC:PG (4:1) membranes without cholesterol, Fig. 5b1–3 displays REDOR-filtered spectra and Fig. 5b4 displays lipid mixing traces of the three constructs. The order of the three constructs in terms of lipid mixing is FP-Hairpin<FP34<N70, and the overall extent of lipid mixing appears smaller than with PC:PG:chol vesicles.

In contrast to the unimodal spectrum of FP34 in PC:PG:chol with peak shift of 174 ppm, the spectrum of FP34 in PC:PG is bimodal with peak shifts of 174 and 178 ppm (Fig. 5b2), which are assigned to protein populations with β-sheet and α-helical Leu7 conformations, respectively. Correlation of FP34 β-sheet population with membrane cholesterol content is apparent from comparison of Fig. 5a2 and b2 and is consistent with earlier SSNMR results on an FP(1–23) fragment.[21] Relative to PC:PG:chol, the spectrum of N70 in PC:PG showed increased intensity of the 178 (helical)-ppm peak, whereas the spectrum of FP-Hairpin showed increased intensity of the 174 (β-sheet)-ppm peak (Fig. 5). The protein:total lipid ratios were a little different between the two membrane compositions. This may be relevant because protein loading has been shown to be positively correlated with the population of β-sheet FP probably because of formation of intermolecular assemblies.[17,21] The effect of protein loading was investigated in Fig. 6, which displays REDOR-filtered Leu7 [13]CO spectra of N70 and FP-Hairpin in PC:PG:chol and PC:PG. Each row in Fig. 6 is for a particular protein and membrane composition with the left and right spectra, respectively, corresponding to lower and higher protein loading. For each spectrum, the relative integrated intensities of the 174 (β-sheet) and 178 (α-helical) peaks are listed in Table 3. For both proteins in both compositions, increased loading is generally correlated with greater population of β-sheet FP. Lipid mixing experiments were also carried out in both compositions for protein:total lipid molar ratios in the range of 1:200 to 1:50. For fusion-active FP34 in PC:PG:chol and N70 in either composition, the final extent of lipid mixing increased approximately linearly with protein loading (data not shown). For N70, the effect of membrane cholesterol can be understood through comparison of the left spectra in the top two rows of Fig. 6, which have similar lower protein loading, and through comparison of the right spectra, which have similar higher loading. For either loading, membrane cholesterol is associated with increased population of β-sheet FP. In some contrast, analogous comparison of the spectra of FP-Hairpin in the third and fourth rows shows that the FP conformation of this construct is approximately independent of membrane cholesterol.

The overall conclusions based on Figs. 4–6 and Tables 2 and 3 are as follows: (1) for either PC:PG:chol or PC:PG, the constructs in terms of lipid mixing function are ordered FP-Hairpin<FP34<N70; (2) populations of membrane-associated protein with either β-sheet or α-helical FP structure are observed; (3) FP34 has the greatest β-sheet population; (4) for all constructs, increased protein loading is generally associated with greater β-sheet and smaller α-helical populations; and (5) for FP34 and N70, greater β-sheet population is positively correlated with membrane cholesterol while for FP-Hairpin, β-sheet and α-helical populations are approximately independent of cholesterol. There is a dramatic functional effect of appending residues C-terminal of the FP region. Adding the NHR (N70) correlates with a large increase in function while adding the NHR and the CHR (FP-Hairpin) results in loss of function. This large variation in function is not obviously correlated with changes in FP conformation. Analysis of the data for the fusion-active FP34 and N70 provides support for the hypothesis that for these constructs, the β-sheet FP conformation is more fusogenic than the α-helical conformation. In particular, there is greater lipid mixing and β-sheet population with either higher protein loading or membrane cholesterol content.

NHR coiled-coil and NHR + CHR SHB regions retain helical structure following membrane association

The dramatic difference between N70 and FP-Hairpin in lipid mixing function is likely related to (1) differential interaction of the NHR with membranes relative to the NHR + CHR and/or (2) differential effect of FP interaction with the membrane due to the NHR *versus* NHR + CHR regions. For either scenario, it is important to have information about the structures of the NHR region of membrane-associated N70 and the NHR + CHR region of membrane-associated FP-Hairpin. In the present study, the S_1 REDOR [13]CO NMR spectrum is correlated with the global conformational distribution of the membrane-associated protein. This spectrum is the sum of equal intensity natural abundance contributions of all of the backbone and side-chain [13]CO nuclei except for the labeled Leu7. There is no lipid contribution because the samples were prepared with ether-linked lipids. As previously described in the article, the backbone [13]CO shift of a residue depends on local conformation; hence, the S_1 spectrum reflects the distribution of conformations of the protein. Figure 7 displays S_1 spectra for the three constructs associated with PC:PG membranes, and these spectra are clearly different from one another. The peak shift of the FP34 spectrum is 174 ppm, while the peak shift of the N70 and FP-Hairpin spectra is 178 ppm. There are shoulders at 178 and 174 ppm in the FP34 and N70 spectra, respectively, and, relative to N70, a smaller 174-ppm shoulder in the FP-Hairpin spectrum. For each construct, an S_1 spectrum of similar appearance was obtained in PC:PG:chol membranes.
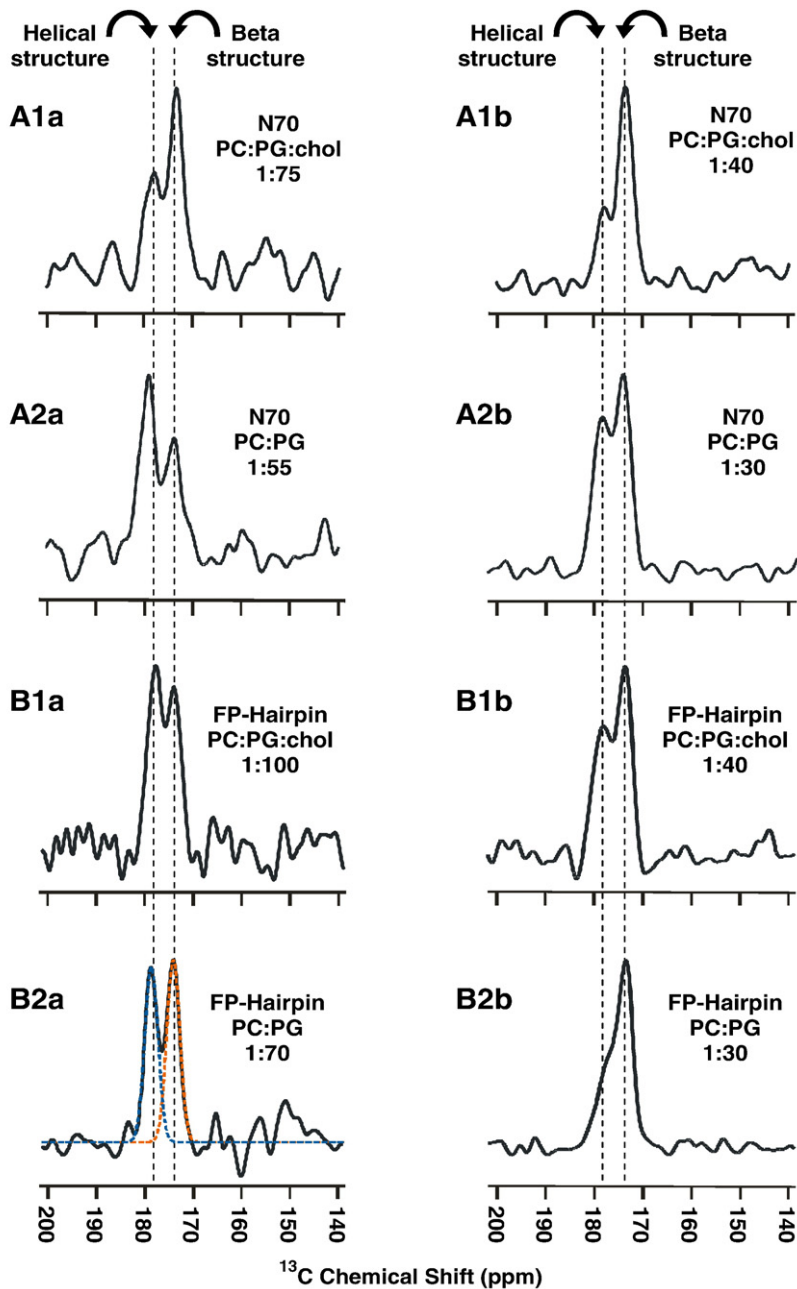
Fig. 6. REDOR difference spectra representing filtered Leu7 ^{13}CO signal for N70 (a1a–a2b) or FP-Hairpin (b1a–b2b) in (a1 and b1) PC:PG:chol or (a2 and b2) PC:PG membranes. The protein:lipid molar ratios are given for each panel and the vertical broken lines are at the peak chemical shifts that are assigned to β-sheet or helical conformation. Each REDOR spectrum represents the sum of (a1a) 107,472, (a1b) 76,832, (a2a) 144,176, (a2b) 54,192, (b1a) 147,120, (b1b) 97,664, (b2a) 101,217, or (b2b) 76,128 $S_0 - S_1$ scans. In spectrum b2a, the orange and blue broken traces are the best-fit deconvolved peaks whose integrated areas were used to determine fractions of β-sheet and helical populations for this sample in Table 3.

For FP(1–23) in β-sheet conformation, the average experimental ^{13}CO shift in the FP region is 174 ppm,[26] and this is reflected in the three FP residues measured in FP34 (Fig. 4 and Table 2). The FP residues make a large contribution to the FP34 S_1 spectrum, and the 174-ppm feature in the S_1 spectra is therefore assigned to β-sheet conformation. The assignment of the 178-ppm feature in FP-Hairpin is based on the DSC data in Fig. 3 and previous CD and high-resolution structural data that are consistent with SHB structure for the NHR+CHR regions with 100% α-helicity.[7–9,18,22] For these residues in helical conformation, the average database backbone ^{13}CO shift is 178 ppm.[33] The NHR+CHR ^{13}COs make the dominant contribution to the FP-Hairpin S_1 spectrum, and the 178-ppm feature in the S_1 spectra is therefore assigned to α-helical confor-

mation. The overall qualitative conclusion from this self-consistent analysis is retention of SHB structure in membrane-associated FP-Hairpin. In addition, detection of a significant 178-ppm peak in the N70 spectrum is consistent with α-helical conformation in the NHR region of N70 that would be expected with retention of the NHR coiled coil.

More quantitative analysis of the S_1 spectra was done by summing individual ^{13}CO signals using distinct secondary-structure models for different regions of the protein: (1) FP and polar region backbone ^{13}COs, β-sheet/strand and helical contributions; (2) NHR and CHR backbone ^{13}COs, helical; and (3) loop backbone ^{13}COs and side-chain ^{13}COs, coil.[33,36] Further details of S_1 spectral modeling are in Experimental Procedures. Figure 7 displays the summed spectra as well as the individual

Table 3. REDOR-filtered Leu7 ^{13}CO chemical shifts for N70 and FP-Hairpin

Protein + (protein:lipid)[a]	Membrane composition	Peak chemical shift (ppm)	Secondary structure[b]	Percentage of area[c]
N70 (1:75)	PC:PG:chol	173.5	β-Sheet	67
		178.0	Helical	33
N70 (1:40)	PC:PG:chol	173.6	β-Sheet	77
		178.2	Helical	23
N70 (1:55)	PC:PG	173.8	β-Sheet	43
		179.0	Helical	57
N70 (1:30)	PC:PG	174.0	β-Sheet	57
		178.6	Helical	43
FP-Hairpin (1:100)	PC:PG:chol	174.3	β-Sheet	47
		178.0	Helical	53
FP-Hairpin (1:70)	PC:PG:chol	173.8	β-Sheet	55
		177.7	Helical	45
FP-Hairpin (1:40)	PC:PG:chol	173.9	β-Sheet	55
		178.3	Helical	45
FP-Hairpin (1:70)	PC:PG	173.9	β-Sheet	53
		178.6	Helical	47
FP-Hairpin (1:30)	PC:PG	173.8	β-Sheet	65
		177.8	Helical	35

[a] Lipid refers to total PC + PG.
[b] Structure is based on the 174.2-ppm peak shift of Leu7 ^{13}CO of β-sheet FP(1–23) and on the database shift distribution of 178.5 ± 1.3 ppm for Leu for helical conformation.[26,33]
[c] Integrated peak areas were determined using deconvolution and a model of two peaks with Gaussian lineshapes. The estimated uncertainty in percentage peak area was ±3% as determined from comparison of different deconvolutions that reasonably fit an experimental spectrum.

contributions from β-sheet/strand, helical, coil, and side-chain signals. The excellent agreement between the experimental and calculated S_1 spectra for FP-Hairpin and FP34 and good agreement for N70 support the structural model and in particular the respective retention of SHB and helical NHR structure in membrane-associated FP-Hairpin and N70. The SHB conclusion is consistent with the hyperthermostable nature of the SHB region of FP-Hairpin (Fig. 3b). The NHR conclusion is consistent with retention of the coiled-coil NHR structure in membrane-associated N70. Coiled-coil NHR structure in N70 would enforce the trimeric FP topology shown in Fig. 1. The formation and significance of this topology are supported by similar rapid rates and large extents of lipid mixing induced by N70 and by a chemically cross-linked FP(1–23) trimer (Fig. 5).[17,21,22] However, this topology likely also exists for FP-Hairpin, which
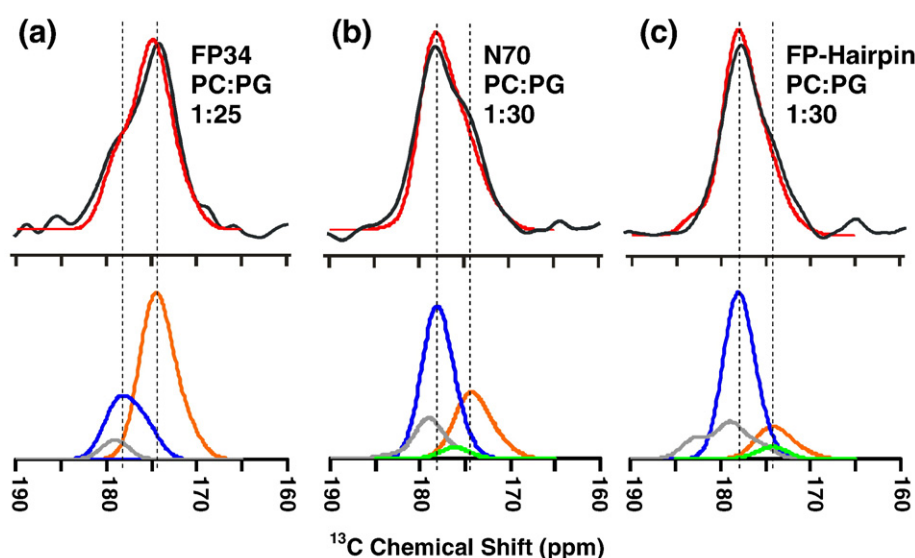

Fig. 7. The black and red traces are, respectively, the experimental and simulated REDOR S_1 ^{13}CO spectra for protein in PC:PG membranes, with protein and experimental protein:lipid molar ratios of (a) 1:25 (FP34), (b) 1:30 (N70), and (c) 1:30 (FP-Hairpin). Each S_1 spectrum represents the sum of contributions from natural abundance ^{13}CO nuclei in the protein, and the area of each simulated spectrum was scaled to that of the corresponding experimental spectrum. The orange, blue, and green traces in the bottom panels are, respectively, the calculated β-sheet/strand, helical, and coil backbone signals, and the gray trace is the side-chain signal. The vertical lines are at the peak simulated ^{13}CO chemical shifts of β-sheet/strand (right) or helical (left) signals.

is both fusion-inactive at physiologic pH and which inhibits fusogens such as FP34 and N70.[22] The SHB structure thus appears to counteract the FP including the highly active trimeric FP topology. It is also possible that fusion requires particular intermolecular FP tertiary structure (for either β-sheet or helical FP conformation) and the more rigid SHB structure may sterically interfere with formation of the appropriate structure.[26]

Connection to earlier studies showing a positive correlation between fusogenicity and FP membrane insertion depth

Because there is no obvious correlation between FP conformational populations and the large differences in fusogenicity between FP34, N70, and FP-Hairpin, other structural determinants of fusogenicity should be considered. Fusogenicity could be affected by regions other than the FP, that is, residues 17–34 of FP34, residues 17–70 of N70, and the SHB region of FP-Hairpin. However, a residue 17–33 gp41 construct is non-fusogenic and the extents of lipid mixing induced by either residue 17–70 or 24–70 gp41 constructs are 10 times less than that of N70.[16,37,38] For fusion-active FP34 and N70, it therefore appears that membrane interactions of the non-FP regions are not major determinants of fusogenicity. The large variation in the fusogenicities of FP34, N70, and FP-Hairpin at physiologic pH might also be related to different oligomeric states. However, solubilization of either N70 or FP-Hairpin in Buffer results in a significant fraction of trimers with some higher-order assembly of trimers driven by the FP region.[18] The respective very high and very low fusion activity of these two constructs is therefore not correlated with their similar oligomeric states. FP34 lacks the NHR trimerization motif and likely aggregates nonspecifically in aqueous solution as evidenced by (1) multiple bands in the gel of an FP34 analog[39] and (2) greater vesicle fusion induced by FP34 initially solubilized in Buffer + non-denaturing detergent compared to FP34 solubilized in Buffer alone.[22] These results could be explained by larger FP34 aggregates in pure aqueous solution, by smaller FP34 oligomers in detergent solution, and by higher fusogenicity of the smaller oligomers as was previously observed for the FP(1–23) construct.[19] For the present study, FP34 was solubilized without detergent, and its putative nonspecific aggregation is different from the assembled trimers of either N70 or FP-Hairpin. However, this distinctive oligomeric state for FP34 does not obviously correlate with FP34 fusogenicity, which was intermediate between that of FP-Hairpin and N70.

The large differences in fusogenicity of FP34, N70, and FP-Hairpin may fit into a structure–function model of different membrane locations of the FP among the three constructs with deeper insertion correlated with greater fusion. This model has strong experimental support from earlier comparative study of three FP(1–23) constructs: V2E mutant monomer, wild-type monomer, and wild-type trimer, which have respective low, moderate, and high fusogenicities, and which are, respectively, on the membrane surface, shallowly inserted, and deeply inserted in PC:PG:chol membranes.[17,21,28] Although most of the existing experimental membrane location data are for the β-sheet FP conformation, there are some data on the α-helical conformation.[21] For either conformation of a particular FP construct, there appear to be similar locations in either membranes or detergent micelles.[21,25,40]

There are clear functional correlations between FP-Hairpin/V2E mutant monomer, FP34/wild-type monomer, and N70/wild-type trimer and there may be structural correlations as well. For both N70 and wild-type trimer in PC:PG membranes at comparable peptide strand:lipid ratios, there is a similar fractional population of molecules with β-sheet FP conformation and a similar population with α-helical conformation (Fig. 6a2).[17,21] The fractional population of molecules with β-sheet FP conformation is positively correlated with membrane cholesterol content (Fig. 6 and Table 3).[21,26] There is also structural similarity between FP34 and wild-type monomer including the cholesterol-dependent conformational populations (Fig. 5a2 and b2).[21] Cholesterol may have an effect on the conformation of the wild-type monomer and trimer because the central regions of both constructs are located in the membrane interior and because cholesterol is primarily located in the membrane interior.[28] The FP conformational populations of FP-Hairpin have little dependence on cholesterol (Fig. 6), which suggests that its FP is not located in the membrane interior. This lack of FP insertion is consistent with both the low fusion activity of FP-Hairpin at physiologic pH (Fig. 5) and the inhibitory effect of FP-Hairpin on FP34- and N70-induced vesicle fusion and suggests that the SHB sequesters the FP from the membrane interior and therefore reduces its membrane perturbation.[22]

In contrast to the negligible lipid mixing induced by Hairpin at pH 7.4, substantial lipid mixing was induced between PC:PS (phosphatidylserine) (3:2) vesicles at pH 3.0 by a construct comprising the NHR, native loop, and CHR regions.[32] A high extent of mixing was also induced between PC:PG:chol (8:2:5) vesicles at pH 3.0 by Hairpin and FP-Hairpin and confirmed that very different lipid mixing results could be obtained at very low non-physiologic pH (K. Sackett and D. P. Weliky, unpublished data). Because of the large number of Glu and Asp residues, the net charge of the CHR region likely changes from negative at pH 7.4 to positive at pH 3.0 (Fig. 2d and e), and this change may affect membrane interaction, particularly for membranes with negatively charged lipids such as PS or PG.

Conclusions

SSNMR structural analysis and lipid mixing functional analysis were carried out for gp41 constructs including N70 and FP-Hairpin, which are models of

the early N-PHI and final SHB gp41 conformations, respectively (Figs. 1 and 2 and Table 1). The NHR region of N70 and NHR and CHR regions of FP-Hairpin retain helical conformation upon membrane association (Fig. 7) and support retention of the respective trimeric coiled-coil and SHB solution structures with corollary support from the hyperthermal stability of the SHB (Fig. 3). Relative to FP34, which has β-sheet FP structure in PC:PG: chol membranes (Fig. 4), there are greater populations of N70 and FP-Hairpin molecules with helical FP structure (Fig. 5). The respective NHR coiled-coil and SHB regions thus have some effect on FP conformational populations that is likely related to trimerization as FP trimers also exhibit greater helicity than do FP monomers.[21] The shorter FP34 contained the FP region but lacked both the NHR and CHR. FP34 served as an FP model for comparison with N70 and FP-Hairpin and for comparison with earlier structural and functional studies on discrete FP fragments such as FP(1–23). The N-PHI model N70 is highly fusogenic at physiologic pH while the SHB model FP-Hairpin is fusion-inactive. The two molecules are similar in forming small assemblies of trimers in aqueous solution and in having populations of membrane-associated molecules with either β-sheet or helical FP conformation. The latter observation can be interpreted to mean that FP conformation is not a major structural determinant of fusogenicity. For both fusion-active FP34 and N70, there is a positive correlation between membrane cholesterol content and larger fractional population of molecules with β-sheet FP conformation, whereas for fusion-inactive and -inhibitory FP-Hairpin, the helical and β-sheet populations are approximately independent of membrane cholesterol (Figs. 5 and 6). Because cholesterol is primarily located in the membrane interior, these observations are consistent with membrane insertion of FP34 and N70 and with lack of insertion of FP-Hairpin. The trimeric coiled-coil NHR structure of a significant fraction of N70 molecules and similar rates and extents of lipid mixing of N70 and an FP trimer support the functional significance of trimeric FP assembly and deep membrane insertion of the FP in the early PHI conformation. Folding to the final SHB conformation could lead to FP withdrawal from the membrane with consequent arrest of membrane perturbation and stabilization of the fused membrane.

Experimental Procedures

Materials

Boc and Fmoc amino acids, Boc MBHA resin, and Fmoc rink amide MBHA resin were purchased from Novabiochem. S-Trityl-β-mercaptopropionic acid was purchased from Peptides International (Louisville, KY). Di-t-butyl-dicarbonate, tris(2-carboxyethyl)phosphine hydrochloride, N-(2-hydroxyethyl)piperazine-N′-2-ethanesulfonic acid (Hepes), and Triton X-100 were purchased from

Sigma. N-(7-Nitro-2,1,3-benzoxadiazol-4-yl)phosphatidyl-ethanolamine, N-(lissamine rhodamine B sulfonyl)phos-phatidylethanolamine, 1-palmitoyl-2-oleoyl-sn-glycero-3-phosphocholine, 1-palmitoyl-2-oleoyl-sn-glycero-3-[phos-pho-rac-(1-glycerol)], 1,2-di-O-tetradecyl-sn-glycero-3-phosphocholine, 1,2-di-O-tetradecyl-sn-glycero-3-phos-pho-rac-(1-glycerol) sodium salt, and cholesterol were purchased from Avanti Polar Lipids, Inc. (Alabaster, AL). Labeled amino acids were purchased from Cambridge Isotopes Labs (Andover, MA) and were Boc-protected using literature methods.[41] The Micro Bicinchoninic Acid protein assay was obtained from Pierce (Rockford, IL). "Buffer" contained 10 or 20 mM formate at pH 3.0 with 200 uM tris(2-carboxyethyl)phosphine hydrochloride.

Peptide synthesis

The sequences (Fig. 2) are based on the HXB2 strain of HIV-1 Envelope protein, as follows: (a) FP34(linker) 512–545-(thioester), (b) FP23(linker) 512–534(S534A)-(thioester), (c) FP34 512–545, and (d) N36(S546C) 546–581. Backbone ^{13}CO (residue i) and ^{15}N (residue $i+1$) isotope labels were incorporated in FP23(linker), FP34(linker), and FP34 for SSNMR analysis. FP34(linker), N36(S546C), FP34, and FP23(linker) were prepared as described previously.[16,18] Synthetic peptides were purified to ~95% purity by reverse-phase high-performance liquid chromatography (RP-HPLC) on C18 or C4 semi-preparative columns using a linear gradient between water/0.1% trifluoroacetic acid and 10% water/90% acetonitrile/0.1% trifluoroacetic acid. Purified peptides were lyophilized and stored at −20 °C under argon. Mass spectroscopy was used to confirm the identity of each purified peptide, and peptide quantification to ±6% accuracy was carried out using a bicinchoninic acid assay.

Protein expression

The gp41 construct N47(L6)C39 (termed Hairpin) corresponding to residues 535(M535C) to 581, followed by a short engineered SGGRGG loop, followed by residues 628 to 666 of HIV-1 HXB2 strain of Envelope protein was expressed and purified as described previously.[22,42] Expression was done in BL-21 cells using the T7 expression system, and following bacteria growth, induction, and protein expression, the centrifuged cell pellet was lysed with glacial acetic acid. After centrifugation, the supernatant was dialyzed against trifluoroacetic acid:water (1:2000 v/v) with 150 μM dithiothreitol, filtered, and concentrated. Hairpin was purified to ~95% homogeneity by RP-HPLC using a C18 preparative column, lyophilized, and stored under argon at −20 °C. Mass spectroscopy confirmed Hairpin identity and Hairpin quantification was based on A_{280} using $\varepsilon = 23,490$ M^{-1} cm^{-1}.

Native chemical ligation

N70 was prepared by ligating FP34(linker) with N36 (S546C) as described previously.[18] The construct N70(L6) C39 (termed FP-Hairpin) was prepared by ligating FP23 (linker) with purified Hairpin at ambient temperature in a solution containing 8 M guanidinium chloride and catalyst, either 30 mM 4-mercaptophenylacetic acid or 30 mM 2-mercaptoethanesulfonic acid, sodium salt.[22,43] Ligation reactions were purified by RP-HPLC using a C4 semi-preparative column with N70 or FP-Hairpin eluting as a well-separated single peak that was identified by mass

spectroscopy. FP-Hairpin was refolded by dialysis into Buffer and stored at 4 °C, while N70 was lyophilized and stored under argon at −20 °C. Quantification was based on the bicinchoninic acid assay (N70) or A_{280} (FP-Hairpin).

Lipid mixing

PC:PG:chol (8:2:5 molar ratio) or PC:PG (4:1) LUVs with ~100 nm diameter were prepared through extrusion in 25 mM Hepes buffer at pH 7.5.[17] A fluorescence assay was used to probe gp41 construct-induced inter-vesicle lipid mixing, which is one feature of vesicle fusion.[22] Ten percent of the LUVs were "labeled" with 2 mol% *N*-(7-nitro-2,1,3-benzoxadiazol-4-yl)phosphatidylethanolamine fluorescent lipid and 2 mol% *N*-(lissamine rhodamine B sulfonyl)phosphatidylethanolamine quenching lipid. Protein-induced fusion with unlabeled vesicles resulted in increased fluorophore–quencher distances and higher fluorescence. The time-resolved change in fluorescence, $\Delta F(t)$, was measured after addition of protein in Buffer and then Triton X-100 was added to completely solubilize the lipids and cholesterol, and the consequent maximum fluorescence change, ΔF_{max}, was calculated as the difference with the initial LUV fluorescence without protein. $\Delta F(t)$ and ΔF_{max} were corrected for the small decrease in fluorescence due to dilution observed when only Buffer was added to the LUV solution. The "percent lipid mixing" or $M(t)$ was calculated using $M(t) = \Delta F(t)/\Delta F_{max} \times 100$. All lipid mixing assays were repeated minimally in triplicate using different batches of LUVs and/or protein. For replicates with the same batches, the typical variation in the long-time value of $M(t)$ was ±2%. For different batches of fusogenic FP34 or N70, the maximum variations were, respectively, ±8% or ±6% and both constructs always exhibited a clear dose response.

Additional experimental details: (1) Fluorescence was measured with a Fluorolog-2 fluorimeter (HORIBA Jobin Yvon, Edison, NJ) under constant stirring at 37 °C. (2) The LUVs were prepared with 1-palmitoyl-2-oleoyl-*sn*-glycero-3-phosphocholine and 1-palmitoyl-2-oleoyl-*sn*-glycero-3-[phospho-*rac*-(1-glycerol)], [PC+PG] = 150 μM, pH 7.5. (3) Acetonitrile was removed from RP-HPLC purified protein either by lyophilization or by extensive dialysis to at least 1:10,000 dilution. (4) Protein was initially dissolved in Buffer at 40 μM polypeptide monomer concentration. Low pH was required to maintain solubility of FP-Hairpin at this concentration. The final LUV+protein solution had [protein] ≤ 4 μM and pH of 7.2–7.3. (5) ΔF_{max} was determined after addition of 12 μL of 10% Triton X-100.

Differential scanning calorimetry

Thermograms were obtained with a Nano II instrument (Calorimetry Sciences Corp., Linden, UT), a 20–125 °C range, and 2°/min ramp. The buffer signal was subtracted from the protein+buffer signal, and the data were analyzed with the program DA-2 from MicroCal, Inc.

NMR sample preparation

The protocol was very similar to that used for the lipid mixing assay. LUVs were prepared with ether-linked 1,2-di-*O*-tetradecyl-*sn*-glycero-3-phosphocholine and 1,2-di-*O*-tetradecyl-*sn*-glycero-3-phospho-*rac*-(1-glycerol) sodium salt lipids, which lack CO nuclei, and with [PC+PG] = 2 mM. Use of ether-linked lipids rather than ester-linked

lipids does not affect FP chemical shifts and presumably FP conformation.[26,35] A 40-μM protein solution in Buffer was added dropwise to the LUV solution for ~1 h under constant stirring, and the pH was maintained above 7.0 with aliquots of 100 mM Hepes, pH 7.4. Dropwise addition reduced protein concentration in solution and favored protein binding to LUVs rather than protein aggregation. The final lipid and protein concentrations were, respectively, 150 and 1.2–6 μM, with 0.1–0.5 μmol total protein used per sample preparation. Proteo-liposome solid material settled during overnight incubation at 4 °C and was further compacted by centrifugation at 4000*g*, transfer to a microtube, and centrifugation at 16,000*g* or 100,000*g*. The pellet was packed in a 4-mm-diameter magic angle spinning (MAS) NMR rotor. Membrane binding by the protein was evidenced by (1) a clear supernatant, (2) $A_{280} \approx 0$ of the supernatants for FP-Hairpin samples, and (3) lack of pelleting of samples containing LUVs but no protein.

Solid-state NMR spectroscopy

Experiments were done on a 9.4-T (400 MHz) spectrometer (Varian Infinity Plus, Palo Alto, CA) using a MAS probe in triple-resonance $^{13}C/^1H/^{15}N$ configuration. The ^{13}C shifts were externally referenced to the methylene resonance of adamantane at 40.5 ppm, which allowed direct comparison with database ^{13}C shifts.[33] Samples were cooled with gas at −50 °C, which does not cause significant structural changes in the protein.[44]

The REDOR pulse sequence was generation of ^{13}C transverse magnetization through cross-polarization (CP) followed by a dephasing period and then ^{13}C detection with ^1H decoupling.[35,45,46] For each sample, an "S_0" and an "S_1" acquisition were obtained and the dephasing periods of both acquisitions had a ^{13}C π pulse at the end of each rotor cycle except for the last cycle. The dephasing period of the S_1 acquisition also had a ^{15}N π pulse at the midpoint of each rotor cycle, and the two π pulses per rotor cycle resulted in attenuation of transverse magnetization of ^{13}Cs directly bonded to ^{15}Ns with consequent reduction of the labeled ^{13}CO signal during the detection period. The labeled ^{13}CO signal was not attenuated for S_0 detection; hence, the $S_0 - S_1$ difference was the labeled ^{13}CO signal; the natural abundance ^{13}C signals were quantitatively filtered out.[19]

The experiments were done with 8.0 kHz MAS frequency and with the ^{13}C transmitter at 153 ppm. Time periods included the following: CP, 1.6 ms; dephasing, 2.0 ms; and recycle delay, 1.0 s. Typical rf field amplitudes were as follows: ^{13}C π, 54 kHz; ^{13}C CP ramp, 58–68 kHz; ^{15}N π, 43 kHz; ^1H π/2 pulse and CP, 50 kHz; ^1H decoupling, 90 kHz. Pulse sequence parameters were optimized with polycrystalline adamantane and *N*-acetyl-leucine (^{15}N, 1-^{13}C, *N*-^{13}C) samples and with a lyophilized helical peptide with backbone ^{13}CO and ^{15}N labels at residues 9 and 13, respectively.[26]

^{13}CO S_1 spectral simulations

Each ^{13}CO signal had a Gaussian lineshape with 1.5 ppm standard deviation that was based on the ~3-ppm linewidths of the Leu7 ^{13}CO spectra of Figs. 4–6. For all constructs, the contribution of each of the 16 FP backbone ^{13}COs was divided into a signal calculated using the experimental β-sheet shift[26] and a signal calculated using the database helical shift.[33] Each of the residue 17–34 backbone ^{13}COs in FP34 and residue 17–30 backbone

[13]COs in N70 and FP-Hairpin also contributed a β-strand and a helical signal based on database shifts. Helical database shifts were used for the backbone [13]COs of the NHR region of N70 and the NHR and CHR regions of FP-Hairpin. Coil database shifts were used for the loop backbone [13]COs of FP-Hairpin and the three C-terminal residues of N70 and for the side-chain [13]COs of all constructs.[33,36] For a particular construct, all of the FP and polar region [13]COs had the same fractional contribution (*f*) of β-sheet/strand signal and the same 1 − *f* contribution of helical signal. For each construct, the *f* parameter was adjusted to give a good fit between the experimental and simulated S_1 spectra and to approximately reflect the experimental fraction of β-sheet conformation in the corresponding filtered Leu7 [13]CO spectrum (Figs. 5b2 and 6a2b and b2b; Table 3). *f* = 0.75 for FP34 and *f* = 0.80 for FP-Hairpin and N70.

Acknowledgements

References

1. Jacobs, A., Garg, H., Viard, M., Raviv, Y., Puri, A. & Blumenthal, R. (2008). HIV-1 envelope glycoprotein-mediated fusion and pathogenesis: implications for therapy and vaccine development. *Vaccine*, **26**, 3026–3035.

2. White, J. M., Delos, S. E., Brecher, M. & Schornberg, K. (2008). Structures and mechanisms of viral membrane fusion proteins: multiple variations on a common theme. *Crit. Rev. Biochem. Mol. Biol.* **43**, 189–219.

3. Markosyan, R. M., Cohen, F. S. & Melikyan, G. B. (2003). HIV-1 envelope proteins complete their folding into six-helix bundles immediately after fusion pore formation. *Mol. Biol. Cell*, **14**, 926–938.

4. Furuta, R. A., Wild, C. T., Weng, Y. & Weiss, C. D. (1998). Capture of an early fusion-active conformation of HIV-1 gp41. *Nat. Struct. Biol.* **5**, 276–279.

5. Bewley, C. A., Louis, J. M., Ghirlando, R. & Clore, G. M. (2002). Design of a novel peptide inhibitor of HIV fusion that disrupts the internal trimeric coiled-coil of gp41. *J. Biol. Chem.* **277**, 14238–14245.

6. Liu, S., Wu, S. & Jiang, S. (2007). HIV entry inhibitors targeting gp41: from polypeptides to small-molecule compounds. *Curr. Pharm. Des.* **13**, 143–162.

7. Chan, D. C., Fass, D., Berger, J. M. & Kim, P. S. (1997). Core structure of gp41 from the HIV envelope glycoprotein. *Cell*, **89**, 263–273.

8. Tan, K., Liu, J., Wang, J., Shen, S. & Lu, M. (1997). Atomic structure of a thermostable subdomain of HIV-1 gp41. *Proc. Natl Acad. Sci. USA*, **94**, 12303–12308.

9. Weissenhorn, W., Dessen, A., Harrison, S. C., Skehel, J. J. & Wiley, D. C. (1997). Atomic structure of the ectodomain from HIV-1 gp41. *Nature*, **387**, 426–430.

10. Chan, D. C. & Kim, P. S. (1998). HIV entry and its inhibition. *Cell*, **93**, 681–684.

11. Freed, E. O., Delwart, E. L., Buchschacher, G. L., Jr. & Panganiban, A. T. (1992). A mutation in the human immunodeficiency virus type 1 transmembrane glycoprotein gp41 dominantly interferes with fusion and infectivity. *Proc. Natl Acad. Sci. USA*, **89**, 70–74.

12. Pereira, F. B., Goni, F. M., Muga, A. & Nieva, J. L. (1997). Permeabilization and fusion of uncharged lipid vesicles induced by the HIV-1 fusion peptide adopting an extended conformation: dose and sequence effects. *Biophys. J.* **73**, 1977–1986.

13. Nieva, J. L. & Agirre, A. (2003). Are fusion peptides a good model to study viral cell fusion? *Biochim. Biophys. Acta*, **1614**, 104–115.

14. Li, Y. & Tamm, L. K. (2007). Structure and plasticity of the human immunodeficiency virus gp41 fusion domain in lipid micelles and bilayers. *Biophys. J.* **93**, 876–885.

15. Reichert, J., Grasnick, D., Afonin, S., Buerck, J., Wadhwani, P. & Ulrich, A. S. (2007). A critical evaluation of the conformational requirements of fusogenic peptides in membranes. *Eur. Biophys. J.* **36**, 405–413.

16. Sackett, K. & Shai, Y. (2002). The HIV-1 gp41 N-terminal heptad repeat plays an essential role in membrane fusion. *Biochemistry*, **41**, 4678–4685.

17. Yang, R., Prorok, M., Castellino, F. J. & Weliky, D. P. (2004). A trimeric HIV-1 fusion peptide construct which does not self-associate in aqueous solution and which has 15-fold higher membrane fusion rate. *J. Am. Chem. Soc.* **126**, 14722–14723.

18. Sackett, K., Wexler-Cohen, Y. & Shai, Y. (2006). Characterization of the HIV N-terminal fusion peptide-containing region in context of key gp41 fusion conformations. *J. Biol. Chem.* **281**, 21755–21762.

19. Yang, J., Prorok, M., Castellino, F. J. & Weliky, D. P. (2004). Oligomeric β-structure of the membrane-bound HIV-1 fusion peptide formed from soluble monomers. *Biophys. J.* **87**, 1951–1963.

20. Bernstein, H. B., Tucker, S. P., Kar, S. R., McPherson, S. A., McPherson, D. T., Dubay, J. W. *et al.* (1995). Oligomerization of the hydrophobic heptad repeat of gp41. *J. Virol.* **69**, 2745–2750.

21. Qiang, W. & Weliky, D. P. (2009). HIV fusion peptide and its cross-linked oligomers: efficient syntheses, significance of the trimer in fusion activity, correlation of β strand conformation with membrane cholesterol, and proximity to lipid headgroups. *Biochemistry*, **48**, 289–301.

22. Sackett, K., Nethercott, M. J., Shai, Y. & Weliky, D. P. (2009). Hairpin folding of HIV gp41 abrogates lipid mixing function at physiologic pH and inhibits lipid mixing by exposed gp41 constructs. *Biochemistry*, **48**, 2714–2722.

23. Dimitrov, A. S., Louis, J. M., Bewley, C. A., Clore, G. M. & Blumenthal, R. (2005). Conformational changes in HIV-1 gp41 in the course of HIV-1 envelope glycoprotein-mediated fusion and inactivation. *Biochemistry*, **44**, 12471–12479.

24. Lu, M., Ji, H. & Shen, S. (1999). Subdomain folding and biological activity of the core structure from human immunodeficiency virus type 1 gp41: implications for viral membrane fusion. *J. Virol.* **73**, 4433–4438.

25. Jaroniec, C. P., Kaufman, J. D., Stahl, S. J., Viard, M., Blumenthal, R., Wingfield, P. T. & Bax, A. (2005). Structure and dynamics of micelle-associated human immunodeficiency virus gp41 fusion domain. *Biochemistry*, **44**, 16167–16180.

26. Qiang, W., Bodner, M. L. & Weliky, D. P. (2008). Solid-state NMR spectroscopy of human immunodeficiency virus fusion peptides associated with host-cell-like membranes: 2D correlation spectra and distance measurements support a fully extended conformation and models for specific antiparallel strand registries. *J. Am. Chem. Soc.* **130**, 5459–5471.

27. Brugger, B., Glass, B., Haberkant, P., Leibrecht, I., Wieland, F. T. & Krausslich, H. G. (2006). The HIV lipidome: a raft with an unusual composition. *Proc. Natl Acad. Sci. USA*, **103**, 2641–2646.

28. Qiang, W., Sun, Y. & Weliky, D. P. (2009). A strong correlation between fusogenicity and membrane insertion depth of the HIV fusion peptide. *Proc. Natl Acad. Sci. USA*, 15314–15319.

29. Sturtevant, J. M. (1987). Biochemical applications of differential scanning calorimetry. *Annu. Rev. Phys. Chem.* **38**, 463–488.

30. Krell, T., Greco, F., Engel, O., Dubayle, J., Dubayle, J., Kennel, A. *et al.* (2004). HIV-1 gp41 and gp160 are hyperthermostable proteins in a mesophilic environment—characterization of gp41 mutants. *Eur. J. Biochem.* **271**, 1566–1579.

31. Jacobs, A., Simon, C. & Caffrey, M. (2006). Thermo-stability of the HIV gp41 wild-type and loop muta-tions. *Protein Pept. Lett.* **13**, 477–480.

32. Lev, N., Fridmann-Sirkis, Y., Blank, L., Bitler, A., Epand, R. F., Epand, R. M. & Shai, Y. (2009). Conformational stability and membrane interaction of the full-length ectodomain of HIV-1 gp41: implica-tion for mode of action. *Biochemistry*, **48**, 3166–3175.

33. Zhang, H. Y., Neal, S. & Wishart, D. S. (2003). RefDB: a database of uniformly referenced protein chemical shifts. *J. Biomol. NMR*, **25**, 173–195.

34. Sackett, K. & Shai, Y. (2005). The HIV fusion peptide adopts intermolecular parallel β-sheet structure in membranes when stabilized by the adjacent N-terminal heptad repeat: a ^{13}C FTIR study. *J. Mol. Biol.* **350**, 790–805.

35. Zheng, Z., Yang, R., Bodner, M. L. & Weliky, D. P. (2006). Conformational flexibility and strand arrange-ments of the membrane-associated HIV fusion pep-tide trimer probed by solid-state NMR spectroscopy. *Biochemistry*, **45**, 12960–12975.

36. Evans, J. N. S. (1995). Biomolecular NMR Spectroscopy Oxford University Press, New York, NY.

37. Peisajovich, S. G., Epand, R. F., Pritsker, M., Shai, Y. & Epand, R. M. (2000). The polar region consecutive to HIV-1 fusion peptide participates in membrane fusion. *Biochemistry*, **39**, 1826–1833.

38. Lev, N. & Shai, Y. (2007). Fatty acids can substitute the HIV fusion peptide in lipid merging and fusion: an analogy between viral and palmitoylated eukaryotic fusion proteins. *J. Mol. Biol.* **374**, 220–230.

39. Pritsker, M., Rucker, J., Hoffman, T. L., Doms, R. W. & Shai, Y. (1999). Effect of nonpolar substitutions of the conserved Phe[11] in the fusion peptide of HIV-1 gp41 on its function, structure, and organization in membranes. *Biochemistry*, **38**, 11359–11371.

40. Morris, K. F., Gao, X. & Wong, T. C. (2004). The interactions of the HIV gp41 fusion peptides with zwitterionic membrane mimics determined by NMR spectroscopy. *Biochim. Biophys. Acta*, **1667**, 67–81.

41. Harris, R. B. & Wilson, I. B. (1984). Tert-butyl aminocarbonate (*tert*-butyloxycarbonyloxyamine)—a new acylating reagent for amines. *Int. J. Pept. Protein Res.* **23**, 55–60.

42. Curtis-Fisk, J., Spencer, R. M. & Weliky, D. P. (2008). Isotopically labeled expression in *E. coli*, purification, and refolding of the full ectodomain of the influenza virus membrane fusion protein. *Protein Expression Purif.* **61**, 212–219.

43. Johnson, E. C. & Kent, S. B. (2006). Insights into the mechanism and catalysis of the native chemical ligation reaction. *J. Am. Chem. Soc.* **128**, 6640–6646.

44. Bodner, M. L., Gabrys, C. M., Parkanzky, P. D., Yang, J., Duskin, C. A. & Weliky, D. P. (2004). Temperature dependence and resonance assignment of ^{13}C NMR spectra of selectively and uniformly labeled fusion peptides associated with membranes. *Magn. Reson. Chem.* **42**, 187–194.

45. Gullion, T. & Schaefer, J. (1989). Rotational-echo double-resonance NMR. *J. Magn. Reson.* **81**, 196–200.

46. Murphy, O. J., III, Kovacs, F. A., Sicard, E. L. & Thompson, L. K. (2001). Site-directed solid-state NMR measurement of a ligand-induced conforma-tional change in the serine bacterial chemoreceptor. *Biochemistry*, **40**, 1358–1366.